Electronic Supplementary Material (ESI) for Journal of Materials Chemistry A.

Trace Level Doping of Lithium-Rich Cathode Materials

Miklos Lengyel[a], *Kuan-Yu Shen*[a], *Deanna M. Lanigan*[a], *Jonathan M. Martin*[b], *Xiaofeng Zhang*[c], *Richard L. Axelbaum*[a*]

[a] Department of Energy, Environmental and Chemical Engineering, Washington University in St. Louis, One Brookings Drive, St. Louis, MO 63130, USA

[b] Permanent address: University of California, Santa Barbara, Lagoon Road, Isla Vista, CA 93117 USA

[c] Chemical Sciences and Engineering Division, Argonne National Laboratory, 9700 South Cass Avenue, Argonne, IL 60439, USA

E-mail address of authors: mlengyel@wustl.edu, shen.k@wustl.edu, dlanigan@go.wustl.edu, j_m_m@umail.ucsb.edu, xfzhang7@gmail.com, axelbaum@wustl.edu

[*] Corresponding author's contact information:

1 Brookings Drive, Campus Box 1180, St. Louis, MO 63130, USA.

Tel: +1-314-935-7560; Fax: +1-314-935-5464.

E-mail address: axelbaum@wustl.edu

REVIEW OF SYNTHESIS METHODS FOR PRODUCING LITHIUM-MANGANESE RICH MATERIALS - Various synthesis methods exist for producing layered cathode materials including co-precipitation, solid-state synthesis, polymer-assisted synthesis, ball milling, combustion synthesis and spray pyrolysis[1-5]. Among these methods, spray pyrolysis allows for a level of control of product purity that is unlikely to be reproduced by any other synthesis method. In spray pyrolysis each droplet acts as a microreactor, thuspreserving the composition of the precursor solution. No additives are required, which allows accurate control of the dopant profile to trace levels in the product.

DOPANT EFFECTS - Substituting Li^+ with an alkali metal may improve the stability of the structure due to steric effects caused by the larger size dopant, as they also carry a single positive charge. Kang and Ceder using computational techniques[6] have shown that Li^+ ion hopping is affected by the size of the tetrahedral vacancy site, and the electrostatic interaction between Li^+ in that site and the cation in the adjacent face sharing octahedron. In general, the screening effect of the original transitional metal ions is very important for the diffusion of Li^+ ions. Therefore, doped samples may have lower diffusivities, where the bonds with oxygen become more polarized due to an increase in electronegativity difference. This is a complicated effect, especially when it is coupled to a change in oxidation state and the dopant does not carry the same theoretical charge (e.g. $Mn^{4+} \leftrightarrow Al^{3+}$).

Replacing Li^+ ions in the interstitial sites with larger alkali metals leads to an increase in the amount of residual ions in the interstitial host sites after charging, because often the dopants do not participate in the intercalation reaction, as reported for Na doping[7]. Kim *et al.* found that Li_xMO_2 based structures have strong driving forces and low energy kinetic paths to transform into spinel structures and that these driving forces do not exist for Na-based counterparts of the

materials[8]. These spinel-transformation reactions are speculated to proceed via transitional metal hopping. The migration of the TM (e.g., Mn) ions has to be coupled with the migration of Li^+ ions, which may become hindered due to the larger size of the Na^+ ions.

Substituting Mn with Al may lead to a slight reduction in the electrochemically active cathode material content of the sample with aluminum having only a single $^{+3}$ oxidation state. Al is similar to Mn in size, and the single oxidation state may be the reason behind the improved stability of Al doped compounds. Several studies demonstrated the beneficial effect of Al on stabilizing the cathode material primarily by creating an Al-coated surface to prevent surface dissolution of the Mn-based active cathode material [9-11]. Additionally, replacing Mn^{+4} with Al^{+3} ions should lead to an increase in the average oxidation state of the Mn ions. To maintain charge neutrality this beneficial effect can mitigate the potentially arising Jahn-Teller distortion effect [12].

Alkali earth metals (Mg, Ca, Sr, Ba) have larger ionic radii than Co^{3+} or Ni^{2+} atoms. Their introduction to the structure has been shown to improve the stability similar to Al and may reduce the capacity reducing the available intercalation sites due to their single +2 oxidation state [13-17]. Substituting Co^{+3} for M^{+2} ions is also expected to increase the average oxidation state of the transitional metal ions originally residing in the structure thereby reducing TM dissolution.

REVIEW OF REVERSIBLE OXYGEN CHEMISTRY – In a conventional description of the oxidation states in a solid compound alkali atoms are anticipated to carry a single, positive charge, alkali earth atoms two positive charges, while oxygen two negative charges. To maintain electroneutrality for $LiCoO_2$, the previously mentioned would require Co to be in a Co^{3+} oxidation state. Earlier several groups [18-21] have shown based upon both experimental observations and computational results that the oxidation state of cobalt remains the same during the intercalation process in $LiCoO_2$, and that the Fermi-level electrons of the material are located

62 at the oxygen atoms. They concluded that the only possible way to maintain charge neutrality
63 would be to require a reversible oxygen chemistry to occur in the $LiCoO_2$ cathode. Furthermore,
64 similar results were obtained for $LiNiO_2$ and its derivatives as well[22, 23]. Recently, this was
65 demonstrated by Sathiya et al.[24] for a Ru and Sn based chemistry, and more recent results by
66 Oishi et al. have indicated the phenomenon to occur in the lithium-rich NMC chemistry[25, 26].

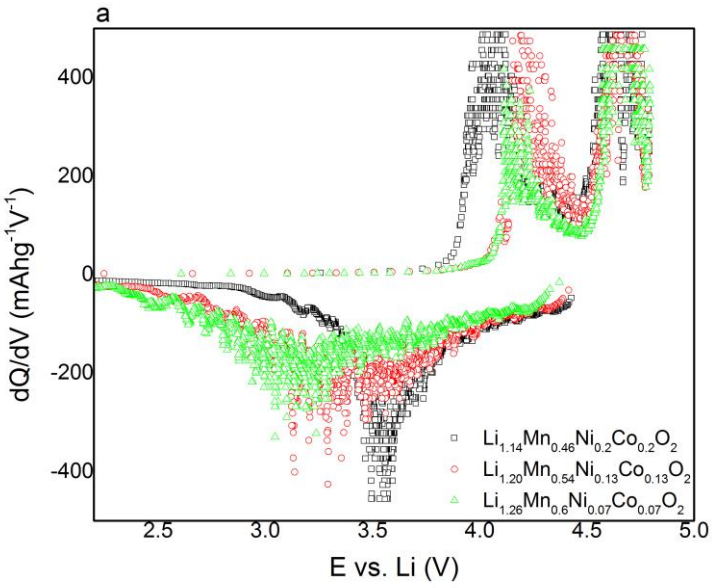

67

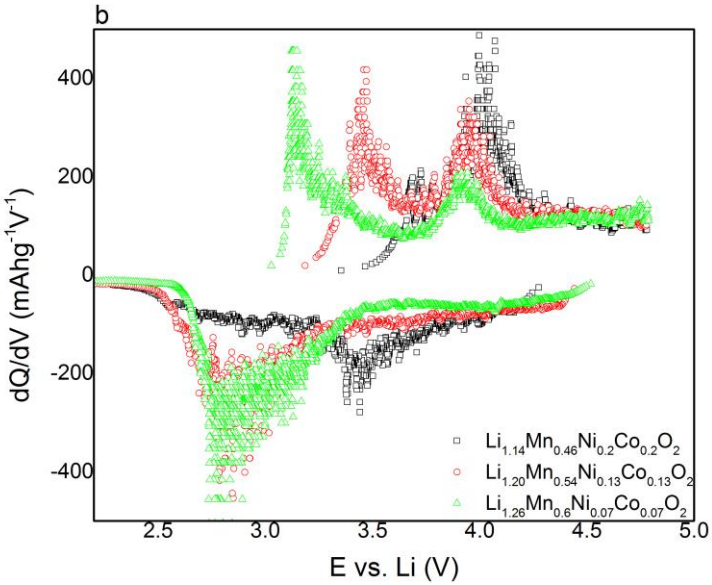

68

69 Fig. S1 - dQ/dV curves of $Li_{1.14}Mn_{0.46}Ni_{0.2}Co_{0.2}O_2$, $Li_{1.2}Mn_{0.54}Ni_{0.13}Co_{0.13}O_2$ and
70 $Li_{1.26}Mn_{0.6}Ni_{0.07}Co_{0.07}O_2$ for (a) cycle 1 and (b) cycle 50.
71

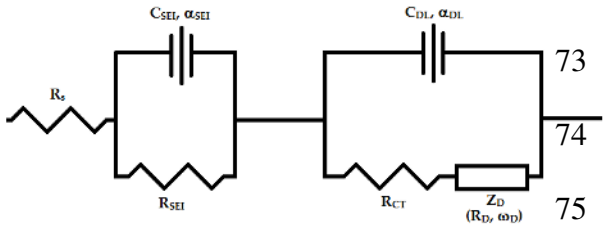

Fig. S2 - The equivalent circuit model used for the interpretation of the EIS spectra.

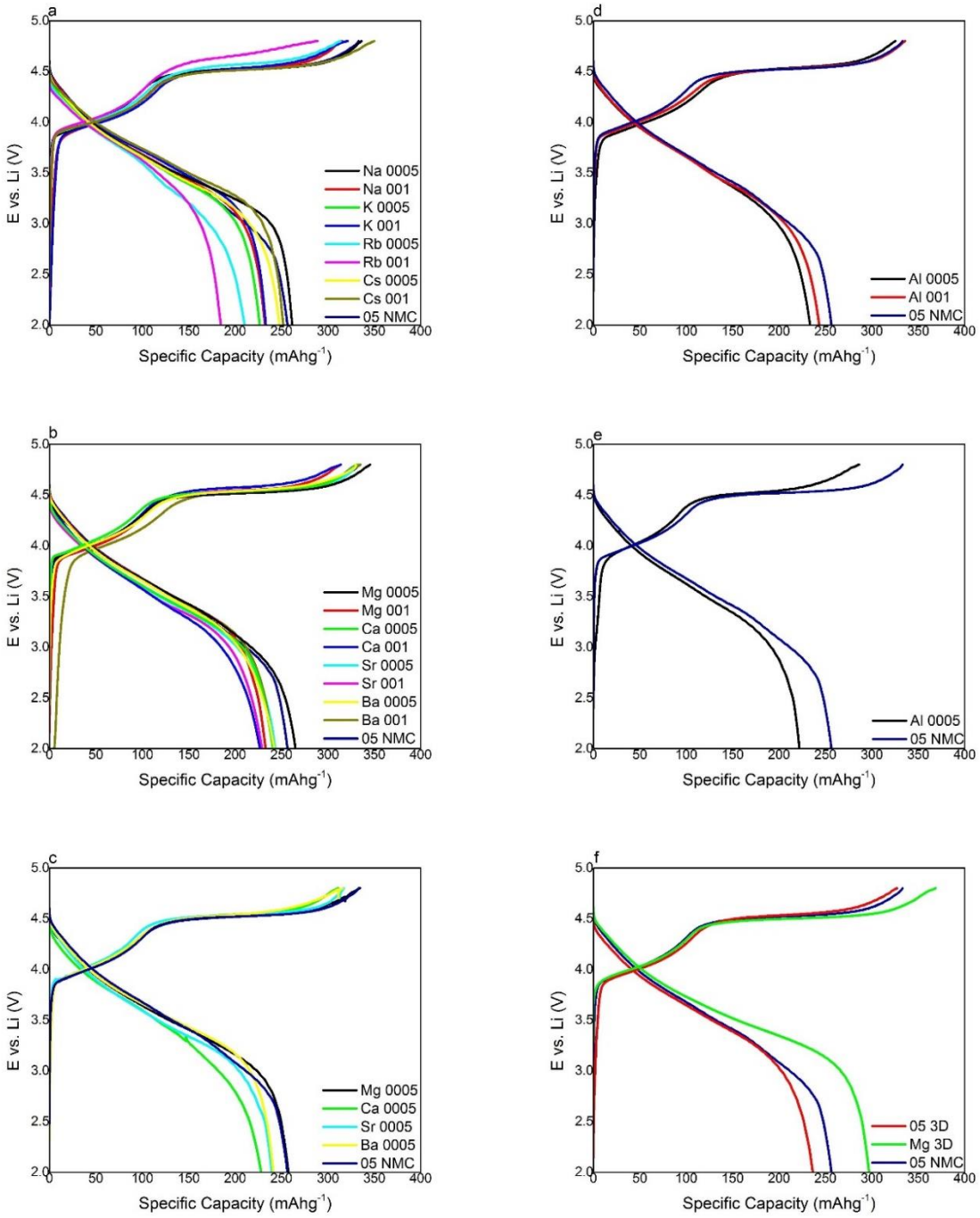

78

79 Fig. S3 - Initial charge and discharge profiles at a constant current density of 20 mAg^{-1} between
80 2.0 and 4.8 V for $Li_{1.2}Mn_{0.54}Ni_{0.13}Co_{0.13}O_2$ samples doped with typically 0.005 or 0.01 level of (a)
81 Na, K, Rb or Cs substituting Li; (b) Mg, Ca, Sr or Ba substituting Co; (c) Mg, Ca, Sr or Ba
82 substituting Ni; (d) Al substituting Mn; (e) Al substituting Ni; (f) $Li_{1.2}Mn_{0.54}Ni_{0.13}Co_{0.13}O_2$ triply
83 substituted with Na, Ba, Al indicated as "05 3D" or Na, Mg, Al indicated as "Mg 3D" at a total
84 dopant level of 0.01 with equal amount of dopant. All materials display two activation-plateaus
85 during the initial charge cycle characteristic of the layered compounds.

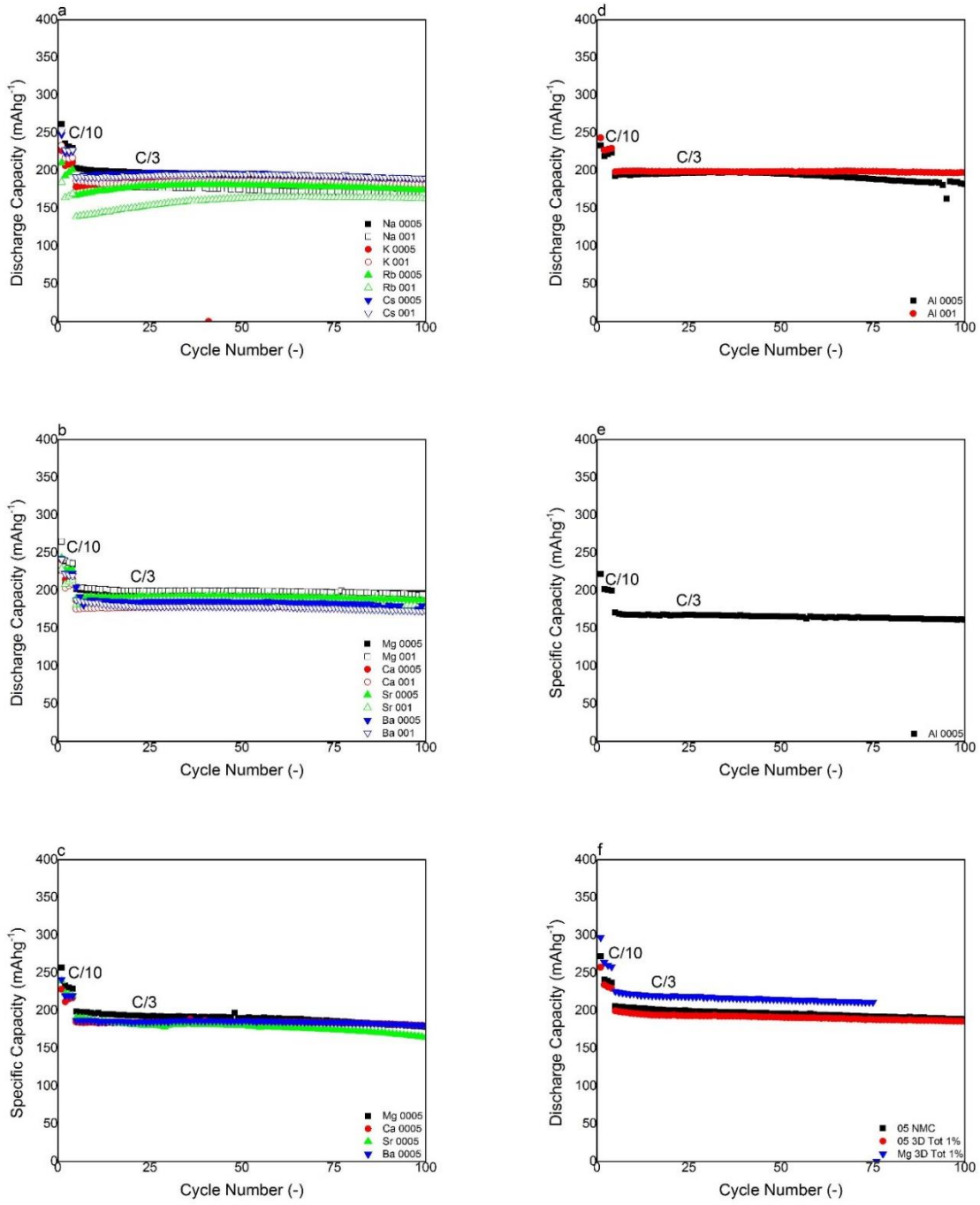

Fig. S4 - Cycling performance of cells doped with (a) 0.005 or 0.01 levels of Na, K, Rb or Cs substituting Li; (b) 0.005 or 0.01 levels of Mg, Ca, Sr or Ba substituting Co; (c) 0.005 Mg, Ca, Sr or Ba substituting Ni; (d) 0.005 or 0.01 level of Al substituting Mn; (e) 0.005 level of Al substituting Ni; (f) $Li_{1.2}Mn_{0.54}Ni_{0.13}Co_{0.13}O_2$ triply substituted with Na, Ba, Al indicated as "05 3D" or Na, Mg, Al indicated as "Mg 3D" at a total dopant level of 0.01 with equal amount of dopant. C/10 equals a current density of 20 mAg^{-1}, while C/3 equals 66.67 mAg^{-1}.

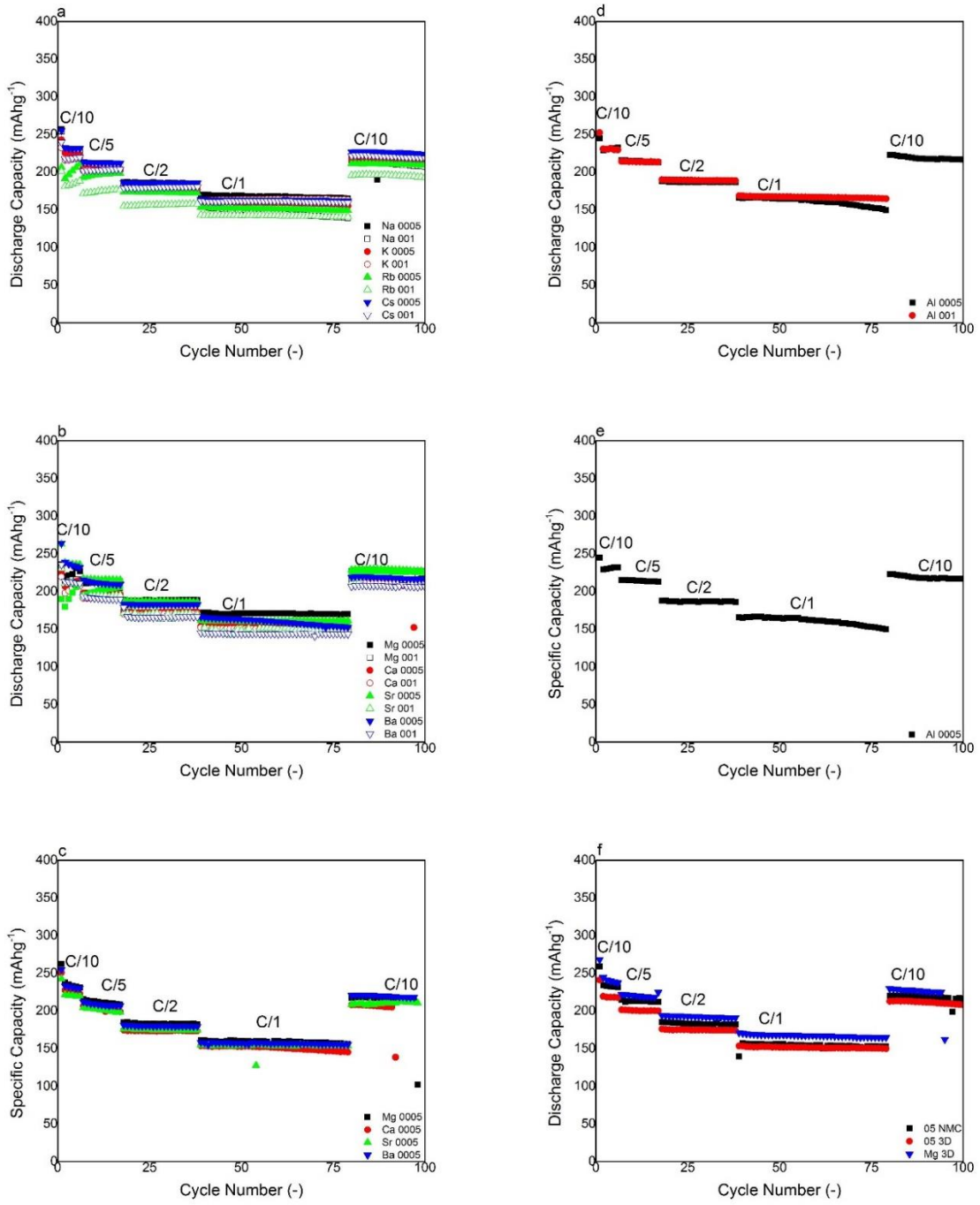

93

94 Fig. S5 – Rate capability test performance of cells doped with (a) 0.005 or 0.01 levels of Na, K,
95 Rb or Cs substituting Li; (b) 0.005 or 0.01 levels of Mg, Ca, Sr or Ba substituting Co; (c) 0.005
96 Mg, Ca, Sr or Ba substituting Ni; (d) 0.005 or 0.01 level of Al substituting Mn; (e) 0.005 level of
97 Al substituting Ni; (f) $Li_{1.2}Mn_{0.54}Ni_{0.13}Co_{0.13}O_2$ triply substituted with Na, Ba, Al indicated as "05
98 3D" or Na, Mg, Al indicated as "Mg 3D" at a total dopant level of 0.01 with equal amount of
99 dopant. C/10, C/5, C/2 and C/1 correspond to a current density of 20, 40, 100, 200 mAg^{-1},
100 respectively.

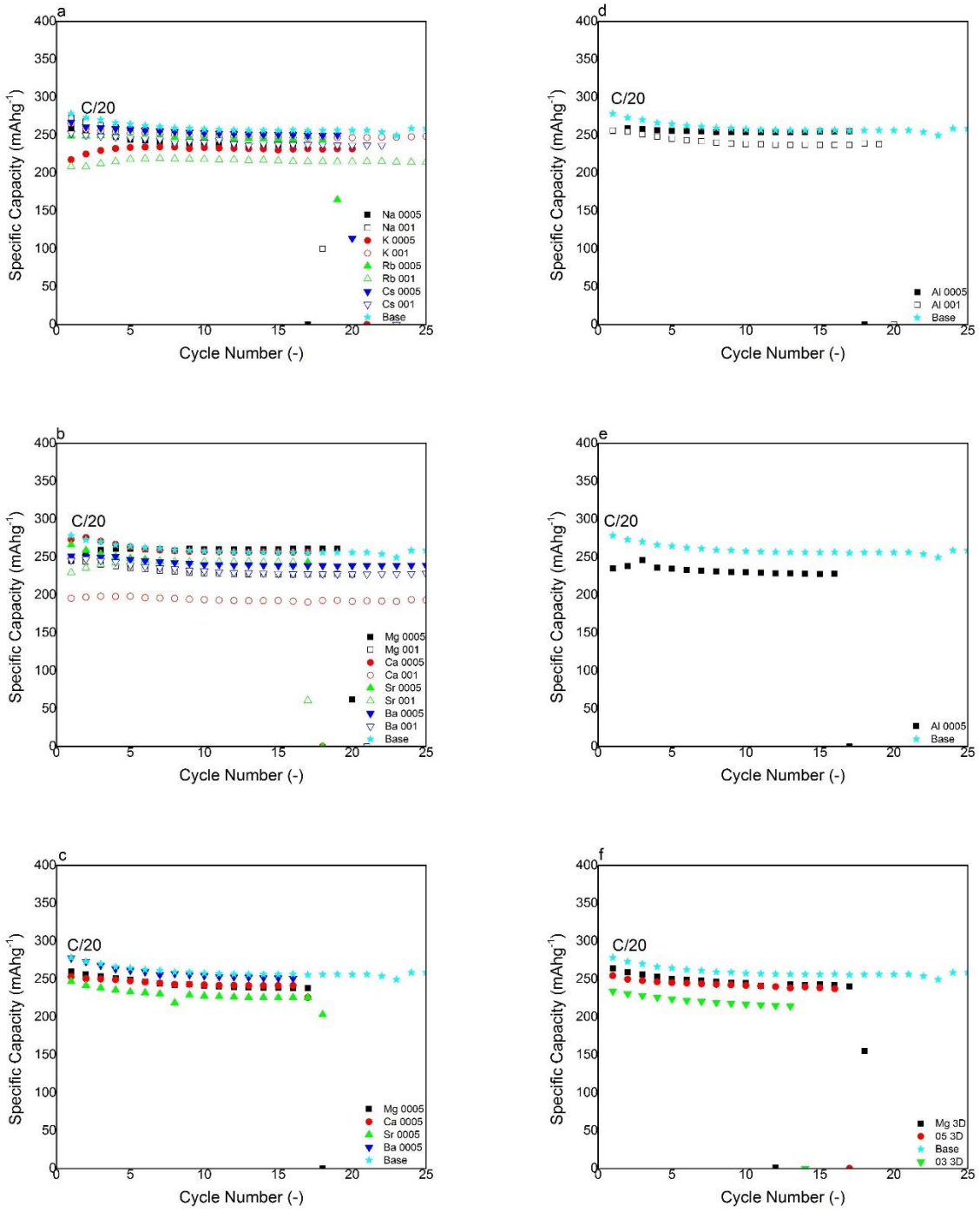

Fig. S6 - Cycling performance of cells doped with (a) 0.005 or 0.01 levels of Na, K, Rb or Cs substituting Li; (b) 0.005 or 0.01 levels of Mg, Ca, Sr or Ba substituting Co; (c) 0.005 Mg, Ca, Sr or Ba substituting Ni; (d) 0.005 or 0.01 level of Al substituting Mn; (e) 0.005 level of Al substituting Ni; (f) $Li_{1.2}Mn_{0.54}Ni_{0.13}Co_{0.13}O_2$ triply substituted with Na, Ba, Al indicated as "05 3D" or Na, Mg, Al indicated as "Mg 3D" at a total dopant level of 0.01 with equal amount of dopant $Li_{1.14}Mn_{0.46}Ni_{0.2}Co_{0.2}O_2$ triply substituted with Na, Ba, Al indicated as "03 3D". The dopant free sample is added to all curves as a teal star for reference.

0.5 NMC				
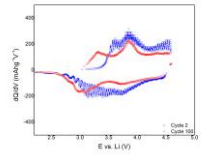				
For Li Na 0005	For Co Mg 0005	For Ni Mg 0005	For Mn Al 0005	For Ni Al 0005
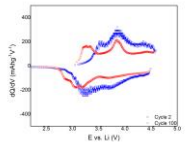	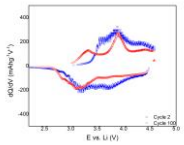	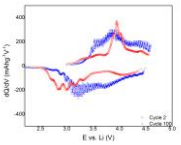	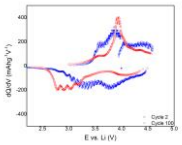	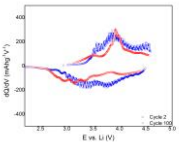
K 0005	Ca 0005	Ca 0005		
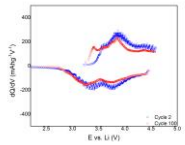	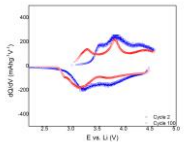	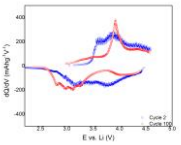		
Rb 0005	Sr 0005	Sr 0005		
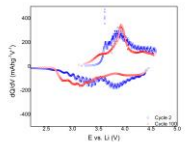	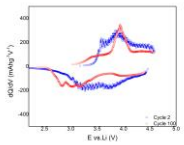	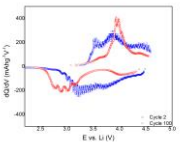		
Cs 0005	Ba 0005	Ba 0005		
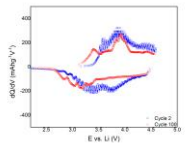	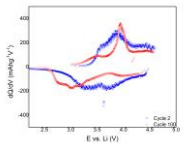	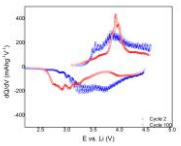		

Fig. S7 – dQ/dV curves of cycle 2 and cycle 100 of the doped samples when cycled at C/3 rate (66.67 mAg^{-1}) between 2.0-4.6 V. The curves are organized according to the position of the dopant element in the periodic table and above each curve the dopant is indicated. All dopant levels in the current table are fixed at 0.005.

Despite the ability of Al to improve capacity retention when substituted for Mn, Al does not appear to reduce the growth of the spinel charge peak that indicates voltage fade. This implies that Al doping improves capacity retention via a different mechanism, for example by reducing the strains along the *c* axis during cycling, as reported for several $LiMn_xO_y$ based spinel materials[27, 28].

0.5 NMC		
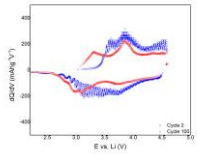		
For Li Na 001	For Co Mg 001	For Mn Al 001
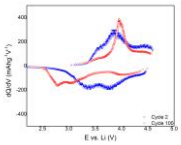	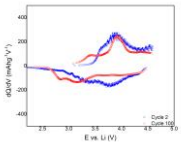	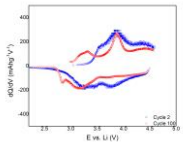
K 001	Ca 001	
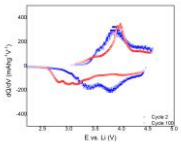	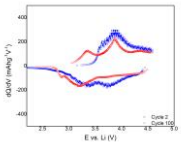	
Rb 001	Sr 001	
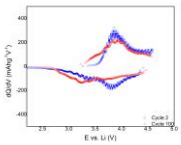	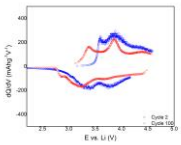	
Cs 001	Ba 001	
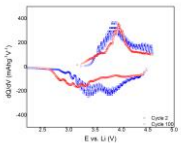	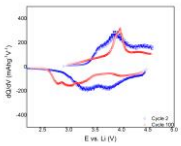	

Fig. S8 - dQ/dV curves of cycle 2 and cycle 100 of the doped samples when cycled at C/3 rate (66.67 mAg^{-1}) between 2.0-4.6 V. The curves are organized according to the position of the dopant element in the periodic table and above each curve the dopant is indicated. All dopant levels in the current table are fixed at 0.01. Ni-doping was omitted from the plot. When compared to the results in Figure S7 it is clear that doubling the dopant levels leads to more significant suppression of the spinel peaks in the charge curves for the alkali and alkali earth metals. Increasing the Al dopant's level for Mn however seems to lead to additional peaks forming in the structure.

128 2.0-4.8 V

0.5 NMC				
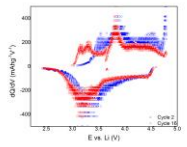				
For Li Na 0005	For Co Mg 0005	For Ni Mg 0005	For Mn Al 0005	For Ni Al 0005
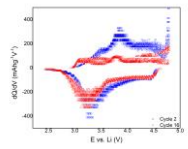	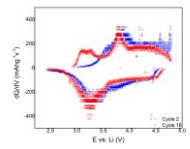	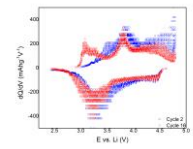	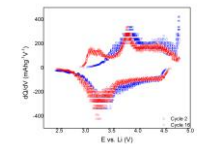	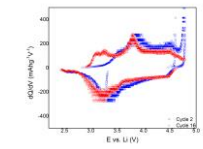
K 0005	Ca 0005	Ca 0005		
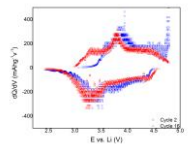	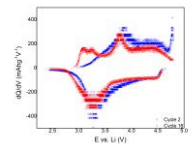	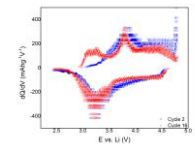		
Rb 0005	Sr 0005	Sr 0005		
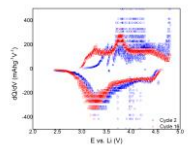	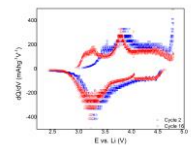	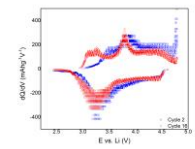		
Cs 0005	Ba 0005	Ba 0005		
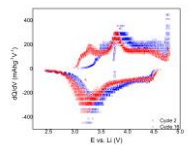	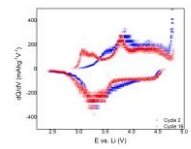	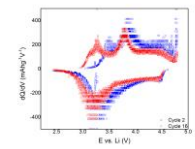		

129 Fig. S9 - dQ/dV curves of cycle 2 and cycle 16 of the doped samples when cycled at C/20 rate
130 (10 mAg^{-1}) between 2.0-4.8 V. All dopant levels in the current table are fixed at 0.005. While
131 improvements can be observed when cycled between 2.0-4.6 V, the dopants have minor effect on
132 the spinel peak growth and peak shift. Additionally, it is clear that all samples still display the
133 original 4.6 V activation peak in the charge profiles at these low currents in cycle 2, which
134 disappears gradually by cycle 16. Similar trends were reported before by Yabuuchi et al.[29] for 0.5
135 NMC, but it is a surprising result for the doped samples.
136

0.5 NMC		
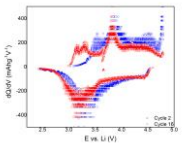		
For Li Na 001	For Co Mg 001	For Mn Al 001
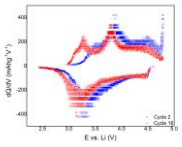	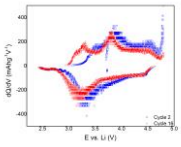	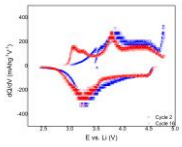
K 001	Ca 001	
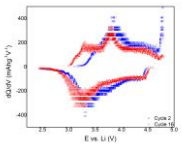	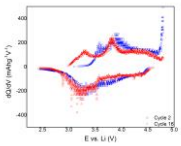	
Rb 001	Sr 001	
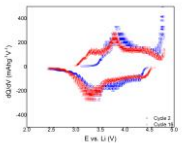	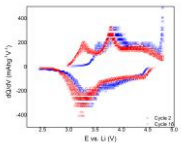	
Cs 001	Ba 001	
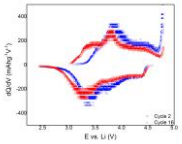	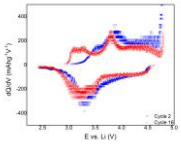	

Fig. S10 - dQ/dV curves of cycle 2 and cycle 16 of the doped samples when cycled at C/20 rate (10 mAg^{-1}) between 2.0-4.8 V. The curves are organized according to the position of the dopant element in the periodic table and above each curve the dopant is included. All dopant levels in the current table are fixed at 0.01.

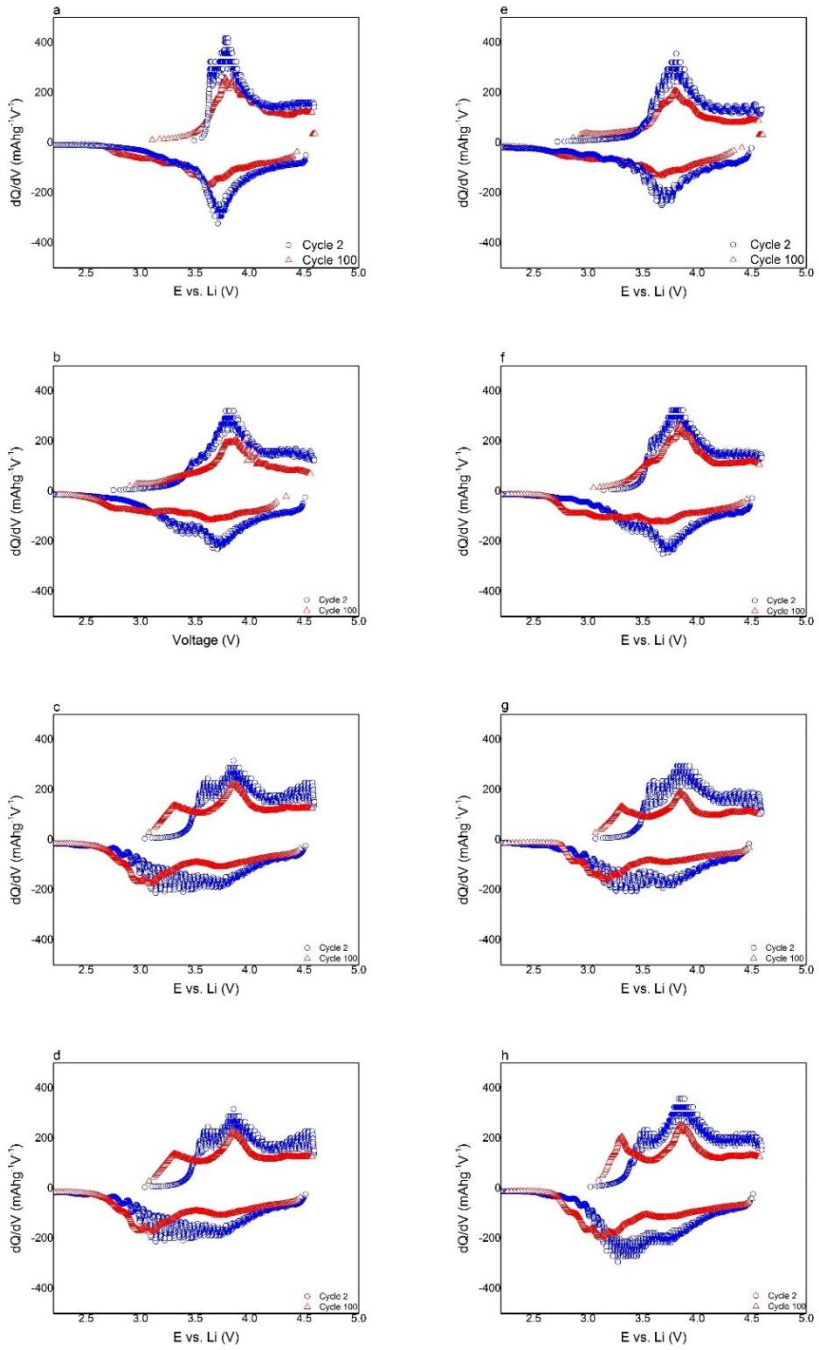

Fig. S11 - dQ/dV curves of cycle 2 and cycle 100 of (a) $Li_{1.09}Mn_{0.43}Ni_{0.24}Co_{0.24}O_2$ (850 °C); (b) $Li_{1.14}Mn_{0.46}Ni_{0.2}Co_{0.2}O_2$ (850 °C); (c) $Li_{1.2}Mn_{0.54}Ni_{0.13}Co_{0.13}O_2$ (900 °C); (d) $Li_{1.2}Mn_{0.54}Ni_{0.13}Co_{0.13}O_2$ (900 °C); (e) $Li_{1.08}Na_{0.01}Mn_{0.42}Al_{0.01}Ni_{0.24}Co_{0.23}Ba_{0.01}O_2$ (800 °C); (f) $Li_{1.13}Na_{0.01}Mn_{0.45}Al_{0.01}Ni_{0.2}Co_{0.19}Ba_{0.01}O_2$ (800 °C); (g) $Li_{1.197}Na_{0.003}Mn_{0.541}Al_{0.003}Ni_{0.13}Co_{0.12}Ba_{0.003}O_2$ (900 °C); (h) $Li_{1.197}Na_{0.003}Mn_{0.541}Al_{0.003}Ni_{0.13}Co_{0.12}Mg_{0.003}O_2$ (900 °C);. The temperatures after the compositions indicate the annealing temperature of the samples. Effects of the annealing temperature on these compositions via spray pyrolysis were reported earlier[30].

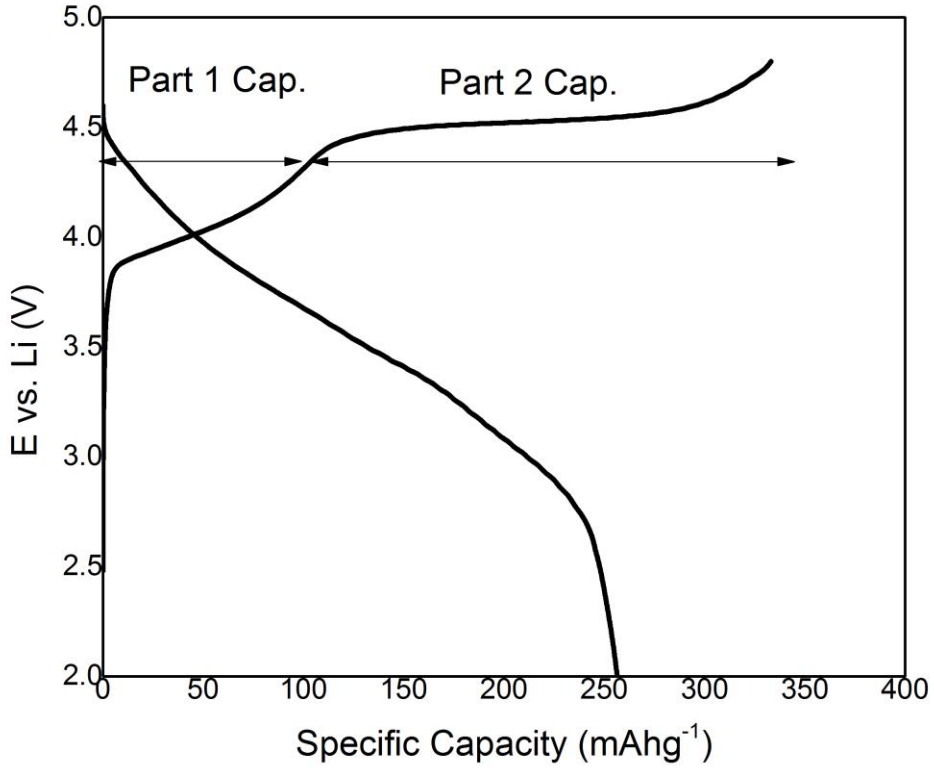

Fig. S12 – A representative first cycle curve displaying the method for estimating capacities in Table S2.

Table S1 - List of doped samples and dopants synthesized in the current study

	Chemical formula	Individual dopant levels
Alkali	$Li_{1.2-x}Na_xMn_{0.54}Ni_{0.13}Co_{0.13}O_2$	0.005, 0.01, 0.025, 0.05, 0.1
	$Li_{1.2-x}K_xMn_{0.54}Ni_{0.13}Co_{0.13}O_2$	0.005, 0.01
	$Li_{1.2-x}Rb_xMn_{0.54}Ni_{0.13}Co_{0.13}O_2$	0.005, 0.01
	$Li_{1.2-x}Cs_xMn_{0.54}Ni_{0.13}Co_{0.13}O_2$	0.005, 0.01
Alkali earth	$Li_{1.2}Mn_{0.54}Ni_{0.13}Co_{0.13-z}Mg_zO_2$	0.005, 0.01, 0.02
	$Li_{1.2}Mn_{0.54}Ni_{0.13}Co_{0.13-z}Ca_zO_2$	0.005, 0.01
	$Li_{1.2}Mn_{0.54}Ni_{0.13}Co_{0.13-z}Sr_zO_2$	0.005, 0.01
	$Li_{1.2}Mn_{0.54}Ni_{0.13}Co_{0.13-z}Ba_zO_2$	0.005, 0.01
	$Li_{1.2}Mn_{0.54}Ni_{0.13-z}Co_{0.13}Mg_zO_2$	0.005
	$Li_{1.2}Mn_{0.54}Ni_{0.13-z}Co_{0.13}Ca_zO_2$	0.005
	$Li_{1.2}Mn_{0.54}Ni_{0.13-z}Co_{0.13}Sr_zO_2$	0.005
	$Li_{1.2}Mn_{0.54}Ni_{0.13-z}Co_{0.13}Ba_zO_2$	0.005
Al	$Li_{1.2}Mn_{0.54-y}Al_yNi_{0.13}Co_{0.13}O_2$	0.005, 0.01
	$Li_{1.2}Mn_{0.54}Al_yNi_{0.13-y}Co_{0.13}O_2$	0.005
Multi-doped samples	$Li_{1.19}Na_{0.01}Mn_{0.53}Al_{0.01}Ni_{0.13}Co_{0.12}Ba_{0.01}O_2$	0.01
	$Li_{1.197}Na_{0.003}Mn_{0.541}Al_{0.003}Ni_{0.13}Co_{0.12}Ba_{0.003}O_2$	0.0033
	$Li_{1.197}Na_{0.003}Mn_{0.541}Al_{0.003}Ni_{0.13}Co_{0.12}Mg_{0.003}O_2$	0.0033
	$Li_{1.13}Na_{0.01}Mn_{0.45}Al_{0.01}Ni_{0.2}Co_{0.19}Ba_{0.01}O_2$	0.01
	$Li_{1.13}Na_{0.01}Mn_{0.45}Al_{0.01}Ni_{0.2}Co_{0.2}O_2$	0.01
	$Li_{1.08}Na_{0.01}Mn_{0.42}Al_{0.01}Ni_{0.24}Co_{0.23}Ba_{0.01}O_2$	0.01
	$Li_{1.08}Na_{0.01}Mn_{0.42}Al_{0.01}Ni_{0.24}Co_{0.24}O_2$	0.01

Table S2 – Capacity of selected doped samples of $Li_{1.2}Mn_{0.54}Ni_{0.13}Co_{0.13}O_2$ with a dopant level of (a) 0.005 and (b) 0.01. 05 3D and Mg 3D stand for a triple doped sample of $Li_{1.2}Mn_{0.54}Ni_{0.13}Co_{0.13}O_2$ with Na, Ba and Al and Na, Mg and Al substituted in a total concentration of 0.01, respectively. The capacities were estimated by measuring the different capacities until the inflection point in the initial charge and discharge curve as indicated in Fig. S12.

a,

	Part 1 Capacity	**Part 2 Capacity**	**Total Capacity**
	$mAhg^{-1}$	$mAhg^{-1}$	$mAhg^{-1}$
Theoretical 05 NMC	**138.9**	**229**	**367.9**
Base	*132*	*225*	*357*
Na	130	207	337
K	130	194	324
Rb	130	185	315
Cs	130	203	333
Al	132	195	327
Mg	150	196	346
Ca	130	202	332
Sr	125	209	334
Ba	132	198	330

b,

	Part 1 Capacity	**Part 2 Capacity**	**Total Capacity**
	$mAhg^{-1}$	$mAhg^{-1}$	$mAhg^{-1}$
Theoretical 05 NMC	**138.9**	**229**	**367.9**
Base	*132*	*225*	*357*
Na	130	186	316
K	130	193	323
Rb	130	170	300
Cs	130	222	352
Al	128	209	337
Mg	110	211	321
Ca	100	216	316
Sr	130	202	332
Ba	120	217	337
05 3D	128	220	348
Mg 3D	128	221	349

Table S3 – Comparison of the effect of different dopants on the rate capability of the doped samples at identical dopant levels and current densities. When Ni is substituted with aluminum vs. Mn substitution the rate capability is considerably inferior at any rate. For alkali earth dopants replacing Ni instead of Co lowers the rate capability of the material, particularly at higher C-rates.

	Cycle 1 @ C/20	**Cycle 1 @ C/10**	**Cycle 1 @ C/5**	**Cycle 1 @ C/2**	**Cycle 1 @ C/1**
Al 0005	255.4	244.6	215.4	187.8	165.7
Ni-Al	235.1	217.0	180.9	156.1	133.3
% Change For Mn-Ni	**108.6**	**112.7**	**119.1**	**120.3**	**124.3**
Mg 0005	244.6	235.7	210.6	188.3	171.9
Ni-Mg	259.9	262.6	215.2	184.4	161.2
% Change For Co-Ni	**94.1**	**89.8**	**97.8**	**102.1**	**106.6**
Ca 0005	273.2	224.6	197.7	172.9	153.9
Ni-Ca	252.9	250.6	206.5	174.5	153.6
% Change For Co-Ni	**108.0**	**89.6**	**95.8**	**99.1**	**100.2**
Sr 0005	266.0	262.8	217.3	187.7	161.5
Ni-Sr	246.8	242.6	204.2	176.0	154.6
% Change For Co-Ni	**107.8**	**108.3**	**106.4**	**106.7**	**104.5**
Ba 0005	251.4	263.7	214.9	183.3	166.2
Ni-Ba	277.5	254.6	212.0	181.2	158.1
% Change For Co-Ni	**90.6**	**103.5**	**101.4**	**101.2**	**105.1**

Table S4 – (a) Observed first cycle charge and discharge capacity and; (b) % capacity lost compared to dopant-free sample.

a,

For Li		Na 0005	K 0005	Rb 0005	Cs 0005	Na 001	K 001	Rb 001	Cs 001
Cycles 1 ($mAhg^{-1}$)	Charge	337.2	324.5	316.0	333.0	316.7	323.5	300.9	352.7
	Discharge	261.5	226.5	210.2	247.8	232.2	233.2	184.6	252.0

For Co		Mg 0005	Ca 0005	Sr 0005	Ba 0005	Mg 001	Ca 001	Sr 001	Ba 001
Cycles 1 ($mAhg^{-1}$)	Charge	346.8	332.4	334.3	330.2	321.3	316.2	332.8	337.3
	Discharge	264.6	240.8	243.2	242.2	226.4	226.8	228.9	241.3

		For Mn Al 0005	For Mn Al 001	05 3D	Mg 3D	03 NMC	03 3D NMC	0.5 NMC
Cycles 1 ($mAhg^{-1}$)	Charge	327.1	338.0	340.4	370.1	328.9	309.0	356.5
	Discharge	233.4	243.3	257.4	296.9	233.9	228.8	271.5

Ni-sub		Mg 0005	Ca 0005	Sr 0005	Ba 0005	Al 0005
Cycles 1 ($mAhg^{-1}$)	Charge	337.6	312.9	318.1	319.0	290.7
	Discharge	257.4	228.0	239.4	241.2	221.9

b,

For Li		Na 0005	K 0005	Rb 0005	Cs 0005	Na 001	K 001	Rb 001	Cs 001
Cycles 1	Charge	5.4	9.0	11.4	6.6	11.2	9.3	15.6	1.1
	Discharge	3.7	16.6	22.6	8.7	14.5	14.1	32.0	7.2

For Co		Mg 0005	Ca 0005	Sr 0005	Ba 0005	Mg 001	Ca 001	Sr 001	Ba 001
Cycles 1	Charge	2.7	6.8	6.2	7.4	9.9	11.3	6.7	5.4
	Discharge	2.5	11.3	10.4	10.8	16.6	16.5	15.7	11.1

		For Mn Al 0005	For Mn Al 001	05 3D	Mg 3D	03 3D NMC	0.5 NMC
Cycles 1	Charge	8.3	5.2	4.5	0.0	6.0	0
	Discharge	14.0	10.4	5.2	0.0	2.2	0

Ni-sub		Mg 0005	Ca 0005	Sr 0005	Ba 0005	Al 0005
Cycles 1	Charge	5.3	12.2	10.8	10.5	18.5
	Discharge	5.2	16.0	11.8	11.1	18.3

References:

1. M. M. Thackeray, S.-H. Kang, C. S. Johnson, J. T. Vaughey, R. Benedek and S. A. Hackney, *J. Mater. Chem.*, 2007, **17**, 3112-3125.
2. W. C. West, J. Soler and B. V. Ratnakumar, *J. Power Sources*, 2012, **204**, 200-204.
3. F. Amalraj, D. Kovacheva, M. Talianker, L. Zeiri, J. Grinblat, N. Leifer, G. Goobes, B. Markovsky and D. Aurbach, *J. Electrochem. Soc.*, 2010, **157**, A1121-A1130.
4. Y. J. Hong, J. H. Kim, M. H. Kim and Y. C. Kang, *Mat. Res. Bull.*, 2012, **47**, 2022-2026.
5. X. Zhang, M. Lengyel and R. L. Axelbaum, *AIChE J.*, 2014, **60**, 443-450.
6. K. Kang and G. Ceder, *Phys. Rev. B*, 2006, **74**, 094105.
7. W. He, D. Yuan, J. Qian, X. Ai, H. Yang and Y. Cao, *J. Mater. Chem. A*, 2013, **1**, 11397.
8. S. Kim, X. Ma, S. P. Ong and G. Ceder, *Phys. Chem. Chem. Phys.*, 2012, **14**, 15571-15578.
9. Y.-K. Sun, S.-W. Cho, S.-W. Lee, C. S. Yoon and K. Amine, *J. Electrochem. Soc.*, 2007, **154**, A168-A172.
10. W. C. West, J. Soler, M. C. Smart, B. V. Ratnakumar, S. Firdosy, V. Ravi, M. S. Anderson, J. Hrbacek, E. S. Lee and A. Manthiram, *J. Electrochem. Soc.*, 2011, **158**, A883-A889.
11. F. Amalraj, M. Talianker, B. Markovsky, L. Burlaka, N. Leifer, G. Goobes, E. M. Erickson, O. Haik, J. Grinblat, E. Zinigrad, D. Aurbach, J. K. Lampert, J.-Y. Shin, M. Schulz-Dobrick and A. Gasuch, *J. Electrochem. Soc.*, 2013, **160**, A2220-A2233.
12. J. Cabana, S.-H. Kang, C. S. Johnson, M. M. Thackeray and C. P. Grey, *J. Electrochem. Soc.*, 2009, **156**, A730-A736.
13. B. V. R. Chowdari, G. V. S. Rao and S. Y. Chow, *Solid State Ionics*, 2001, **140**, 55-62.
14. R. Pelosato, C. Cristiani, G. Dotelli, S. Latorrata, R. Ruffo and L. Zampori, *J. Power Sources*, 2010, **195**, 8116-8123.
15. W. Luo, F. Zhou, X. Zhao, Z. Lu, X. Li and J. R. Dahn, *Chem. Mater.*, 2010, **22**, 1164-1172.
16. W. Chung, H. Jung, C. H. Lee and S. H. Kim, *Thin Solid Films*, 2013, **546**, 98-103.
17. A. H. Tavakoli, H. Kondo, Y. Ukyo and A. Navrotsky, *J. Electrochem. Soc.*, 2013, **160**, A302-A305.
18. P. Kuiper, G. Kruizinga, J. Ghijsen, G. A. Sawatzky and H. Verweij, *Phys. Rev. Lett.*, 1989, **62**, 221.
19. M. Abbate, F. M. F. d. Groot, J. C. Fuggle, A. Fujimori, Y. Tokura, Y. Fujishima, O. Strebel, M. Domke, G. Kaindl, J. v. Elp, B. T. Thole, G. A. Sawatzky, M. Sacchi and N. Tsuda, *Phys. Rev. B*, 1991, **44**, 5419.
20. L. A. Montoro, M. Abbate and J. M. Rosolen, *J. Electrochem. Soc.*, 2000, **147**, 1651-1657.
21. J. Graetz, A. Hightower, C. C. Ahn, R. Yazami, P. Rez and B. Fultz, *J. Phys. Chem. B*, 2001, **106**, 1286-1289.
22. Y. Uchimoto, H. Sawada and T. Yao, *J. Power Sources*, 2001, **97-98**, 326-327.
23. Y. Koyama, Y.-S. Kim, I. Tanaka and H. Adachi, *J. Appl. Phys.*, 1999, **38**, 2024-2027.
24. M. Sathiya, G. Rousse, K. Ramesha, C. P. Laisa, H. Vezin, M. T. Sougrati, M.-L. Doublet, D. Foix, D. Gonbeau, W. Walker, A. S. Prakash, M. B. Hassine, L. Dupont and J.-M. Tarascon, *Nat. Mater.*, 2013, **12**, 827.

25. M. Oishi, C. Yogi, I. Watanabe, T. Ohta, Y. Orikasa, Y. Uchimoto and Z. Ogumi, *J. Power Sources*, 2015, **276**, 89-94.
26. T. Ohzuku, M. Nagayama, K. Tsuji and K. Ariyoshi, *J. Mater. Chem.*, 2011, **21**, 10179.
27. T. E. Conry, A. Mehta, J. Cabana and M. M. Doeff, *Chem. Mater.*, 2012, **24**, 3307-3317.
28. T. E. Conry, A. Mehta, J. Cabana and M. M. Doeff, *J. Electrochem. Soc.*, 2012, **159**, A1562-A1571.
29. N. Yabuuchi, K. Yoshii, S.-T. Myung, I. Nakai and S. Komaba, *J. Am. Chem. Soc.*, 2011, **133**, 4404-4419.
30. M. Lengyel, X. Zhang, G. Atlas, H. L. Bretscher, I. Belharouak and R. L. Axelbaum, *J. Electrochem. Soc.*, 2014, **161**, A1338-A1349.
31. D. Mohanty, S. Kalnaus, R. A. Meisner, K. J. Rhodes, J. Li, E. A. Payzant, D. L. W. III and C. Daniel, *J. Power Sources*, 2013, **229**, 239-248.